

ATP-sensitive potassium channels in the sinoatrial node contribute to heart rate control and adaptation to hypoxia

Qadeer Aziz¹, Malcolm Finlay¹, David Montaigne³, Leona Ojake¹, Yiwen Li¹, Naomi Anderson¹,
Andreas Ludwig² and Andrew Tinker¹ #

¹ - The Heart Centre, William Harvey Research Institute, Barts and the London School of Medicine and Dentistry, Charterhouse Square, London, EC1M 6BQ, UK

² - Institut für Experimentelle und Klinische Pharmakologie und Toxikologie, Universität Erlangen-Nürnberg, Fahrstr. 17, 91054 Erlangen, Germany

³ - Department of Clinical Physiology & Echocardiography, CHU Lille & University of Lille, EGID, Inserm UMR1011, F-59000 Lille, France

Short Title: K_{ATP} in the sinoatrial node

#Corresponding Author. a.tinker@qmul.ac.uk, Tel: 02078825783 Fax: 02078823408, The Heart Centre, William Harvey Research Institute, Barts and the London School of Medicine and Dentistry, Queen Mary University of London, Charterhouse Square, London, EC1M 6BQ, UK.

Keywords: heart rate, sinoatrial node, ion channel, potassium channel, ATP sensitive, hypoxia

ABSTRACT

ATP-sensitive potassium channels (K_{ATP}) contribute to membrane currents in many tissues, are responsive to intracellular metabolism, and open as ATP falls and ADP rises. K_{ATP} channels are widely distributed in tissues and are prominently expressed in the heart. They have generally been observed in ventricular tissue, but they are also expressed in the atria and conduction tissues. In this study, we focused on the contribution and role of the inwardly rectifying K_{ATP} channel subunit, Kir6.1, in the sinoatrial node (SAN). To develop a murine, conduction-specific Kir6.1 KO model, we selectively deleted the Kir6.1 in the conduction system in adult mice (cKO). Electrophysiological data in single SAN cells indicated that Kir6.1 underlies a K_{ATP} current in a significant proportion of cells and influences early repolarization during pacemaking, resulting in prolonged cycle length. Implanted telemetry probes to measure heart rate and electrocardiographic characteristics revealed that the cKO mice have a slow heart rate, with episodes of sinus arrest in some mice. The PR interval was increased, suggesting effects on the atrioventricular node. *Ex vivo* studies of whole

heart or dissected heart regions disclosed impaired adaptive responses of the SAN to hypoxia, and this may have had long-term pathological consequences in the cKO mice. In conclusion, Kir6.1-containing K_{ATP} channels in the SAN have a role in excitability, heart rate control, and the electrophysiological adaptation of the SAN to hypoxia.

INTRODUCTION

ATP sensitive potassium channels (K_{ATP}) contribute to membrane currents in a number of tissues. They are opened by falling cellular ATP and/or rising ADP levels and are important metabolic sensors (1). Substantial K_{ATP} currents were first described in cardiomyocytes and then subsequently in pancreatic beta cells, skeletal muscle, smooth muscle cells and neurones (2,3). K_{ATP} channels are critical in mediating a number of physiological processes. For example, they are central in stimulus secretion coupling underlying insulin release from the endocrine pancreas (4). At the molecular level the channel is a hetero-octamer of four sulphonylurea receptors (SUR1, SUR2A) and four pore forming inwardly rectifying Kir6.0 subunits (Kir6.1, Kir6.2) (5-7). Recent ground

breaking structural studies using cryo-electron microscopy have suggested models for how the channels are able to sense nucleotides at the molecular level (8,9).

Ironically, despite the initial description of the K_{ATP} current in cardiomyocytes and the substantial current density in ventricular cells, it is less clear as to the physiological role this channel plays in cardiac function (1). Mice with global genetic deletion of Kir6.2, which is thought to underlie ventricular cardiac K_{ATP} currents, have impaired exercise tolerance and cardiac performance under sympathetic stimulation suggesting a role in adaptation of the myocyte to the metabolic demands of exercise (10). Furthermore, K_{ATP} currents are present in other chambers in the heart including the atria and conduction system (11,12). Indeed these currents may have unique subunit composition and properties.

The sinoatrial node (SAN) is the dominant pacemaker in the mammalian heart and has unique electrophysiological characteristics underlying this role. There have been few studies on K_{ATP} currents in these cells but it is clear they exist and may at least partially be based upon Kir6.2 subunit expression (13). However Kir6.1 containing channels may also have a role. Global Kir6.1 knockout mice die prematurely from SAN failure and heart block. Initially this was attributed to loss of K_{ATP} channels in coronary vascular smooth muscle leading to vasospasm and cardiac ischaemia (14). However, we have generated mice in which it is possible to selectively delete Kir6.1 in various tissues and at various times using cre/loxP technology (15,16). Mice with deletion in vascular smooth muscle or endothelium do not recapitulate this phenotype suggesting there may be a direct role for Kir6.1 containing K_{ATP} channels in the conduction system (15,16). In this study we explore this idea by using cre/loxP technology using our previously described mice and crossing them with a cre recombinase murine line that allows selective deletion in the cardiac conduction system after the administration of tamoxifen (17)

RESULTS

Generation of the conduction-specific Kir6.1 KO mouse - HCN4cre⁺ Kir6.1(flx/flx) (cKO) mice were generated by crossing Kir6.1(flx/flx) mice with a conduction system-specific cre into which the tamoxifen-inducible Cre-ER^{T2} had been ‘knocked-in’ into the HCN4 locus (see Methods and Figure 1A) (15,16) (17). PCR confirms the presence of cre recombinase (900 bp) at the genomic level in ear tissue from HCN4cre⁺ Kir6.1(flx/flx) mice but not in that of control animals (WT) (Figure 1B). The “floxed” allele is recognised by a PCR reaction spanning exon1, the 5’ loxP site and the recombined FRT site and associated sequence. In the “floxed” mouse this leads to a 600 bp product whilst it generates a 474 bp product in the WT allele (which does not include these additional sequence elements) (Figure 1B). The occurrence of the recombination event in HCN4cre⁺ Kir6.1(flx/flx) mice selectively in the SAN following tamoxifen induction was confirmed using PCR on genomic DNA isolated from SAN, atria and ventricles (Figure 1B).

To confirm the reduced expression of Kir6.1 (Kcnj8) in the SAN of cKO mice, quantitative real-time PCR was used on RNA isolated from SAN, atria and ventricles from cKO and littermate controls post-tamoxifen administration (Figure 1C). Kir6.1 expression was reduced by ~50% in SAN of cKO mice compared to WT SAN (n=5, P<0.01). Expression of Kir6.1 was unaffected in both atria and ventricles confirming conduction system-specific deletion (P>0.05). Interestingly, expression of Kir6.2 (Kcnj11) in SAN was increased by ~50% suggesting possible compensation for Kir6.1 deletion (n=5, P<0.01). SUR1 (Abcc8) and SUR2 (Abcc9) expression was unchanged in any of the cKO tissues assayed compared to WT (n=5, P>0.05).

Kir6.1 deletion reduces the K_{ATP} current in acutely-isolated SAN cells from cKO mice - To investigate if the deletion of Kir6.1 in the SAN has functional consequences, we subjected acutely isolated SAN cells from cKO and WT mice to whole-cell patch clamping (Figure 2). The K_{ATP} current in the SAN has not been extensively characterised so some basic pharmacological experiments were first performed. Not all SAN cells were found to

express a pinacidil/diazoxide-sensitive current (15/29 cells, n=29 cells from 6 mice). Of the WT cells that did express a K_{ATP} current, ~7 % were responsive to pinacidil whilst ~41% were activated by diazoxide (Figure 2). In cells from cKO mice, ~4% and ~11% responded to pinacidil and diazoxide, respectively, (n=28 cells from 4 mice, P=0.015 for diazoxide sensitivity when compared to WT). Both pinacidil and diazoxide sensitive currents were inhibited by tolbutamide. These data suggest that a K_{ATP} channel comprising Kir6.1 is present in a proportion of SAN cells and that it is predominantly activated by diazoxide and inhibited by tolbutamide.

Kir6.1 cKO mice have a bradycardic phenotype - The potential physiological consequences of Kir6.1 deletion in SAN on heart rate and rhythm were then studied. ECG radio-telemetry was used in conscious freely-moving WT and cKO mice (Figure 3). Both WT and cKO mice showed a diurnal variation in heart rate before and after tamoxifen induction (P< 0.01 compared night to day). HR, RR and PR interval were not significantly different before and after tamoxifen administration in ECG recordings from littermate control mice (n=5, P>0.05). Conversely, cKO mice developed a bradycardic phenotype following administration of tamoxifen with significant changes in HR, PR and RR interval both during the day and night (n=8, P>0.05). HR decreased by ~50 bpm during the day and at night and this was reflected in an increase in both RR and PR intervals. A closer investigation of the ECG recordings revealed a much more severe bradycardic phenotype in 3/8 cKO mice (Figure 3E). In these mice, there were pronounced bradycardic episodes with evidence of sinus pauses reflected in RR intervals of greater than 1 second in some instances. We quantified these episodes by counting the number of RR intervals greater than 200 ms in all mice following tamoxifen induction (Figure 3F). cKO mice had a greater frequency of prolonged beats compared to WT mice (P<0.01).

The change in heart rate in cKO mice was further investigated by carrying out heart rate variability (HRV) analysis (Figure 4). We looked at ECG recordings during a period of

low activity (12-2pm) to analyse possible changes in autonomic influence in HRV. Frequency domain analysis showed no change in HRV in WT and cKO mice following tamoxifen induction (n=5, P>0.05). There was no change in the power of both low (0.4-1.5 Hz) and high (1.5-4 Hz) frequency spectra or the total power suggesting that the deletion of Kir6.1 from the conduction system does not grossly affect autonomic control of heart rate.

Action potential duration is prolonged in isolated SAN cells from cKO mice - The effects of conduction-specific Kir6.1 deletion on spontaneous SAN action potentials were investigated using current-clamp (Figure 5). Deletion of Kir6.1 reduced the firing rate of spontaneous action potentials in cKO SAN cells but did not change SAN cell resting membrane and maximum diastolic potential (Figure 5 and Table 1). Initial upstroke velocity was unchanged but time-to-peak was increased in cKO mice (n=11-15 cells from 7-9 mice, P<0.05). Repolarisation was delayed throughout the action potential but particularly during early repolarisation (Figure 5). This was reflected in a ~50% decrease in the action potential duration (APD) ratio, APD₉₀/50 (P<0.005) and an increase in the APD₃₀-40/APD₇₀-80 ratio (P<0.05) in SAN cells from cKO mice (Figure 5F and G). These data suggest that deletion of Kir6.1 changes the duration and shape of the SAN action potential but does not contribute significantly to resting membrane potential in these cells.

To investigate the phenotype further *in-vitro*, MEAs were used to measure spontaneous field potentials in SAN/atrial preparations from WT and cKO mice (Figure 6A and B). MEA recordings showed a significantly reduced beating frequency in preparations from cKO mice compared to WT mice (n=12, P<0.05). In support of these observations, SAN cells acutely isolated from cKO mice after tamoxifen administration have a lower beat frequency (Figure 5B). Both these *ex-vivo* studies indicate that the observed bradycardia in *in-vivo* experiments results from properties intrinsic to the SAN myocytes following deletion of Kir6.1.

Sinus node recovery time (SNRT) is prolonged and its adaptation to stress is compromised in cKO mice - To analyse SAN function in the

intact heart we used a flexMEA to measure the SNRT in the Langendorff-perfused heart (Figure 6C-E). SNRT, following pacing with S1-S1 intervals of 100 ms, was significantly increased in cKO mouse hearts compared to WT hearts (n=10-12, P<0.05) suggesting potential SAN dysfunction in cKO mice. K_{ATP} channels are known to be protective against metabolic challenge (1). To investigate if deletion of Kir6.1 in the SAN changes adaptation to stress, we challenged WT and cKO hearts with hypoxia (Krebs bubbled with 95% N₂/5% CO₂) and measured the SNRT. In WT hearts SNRT was increased following 10 minutes of hypoxia (Figure 6E, P<0.05 compared to control). Interestingly, hypoxia had no effect on SNRT in cKO hearts (P>0.05). SNRT of WT hearts returned close but not completely to basal levels following 10 minutes of reperfusion.

Increased expression of pro-fibrotic markers in hypomorphic cKO SANs - We examined whether deletion of Kir6.1 in the SAN had long-term consequences for SA node morphology and pathology. Masson's trichrome staining was used to investigate if Kir6.1 deletion increases fibrosis and changes the morphology of the SAN in cKO mice (Figure 7). The SA node appeared smaller and thinner in SAN sections from cKO mice, with fewer viable myocytes. There was more fibrous tissue compared to WT SANs. To quantify these observations RT-qPCR was performed for known fibrosis-related genes. An increase in expression of a number of pro-fibrotic markers within cKO SANs was observed (Figure 7C). Specifically, the expression of genes for collagen (Colla3), Tgf-β1 and Tgf-β2 were significantly increased by ~50 % (n=5, P<0.05). These data suggest that deletion of Kir6.1 in the SAN can lead to an increase in pro-fibrotic markers and fibrosis. We also examined if there were any changes in expression of ion channels other than Kir6.1 in the cKO mice indicative of a remodelling process. We used RT-qPCR (n=4 mice, mean from triplicate measurements of ΔC_T) to measure the expression of Hcn4 (WT7.73±0.46; cKO 7.52±0.16), Hcn1 (WT8.77±0.28; cKO 7.70±0.62), Kcnj3 (WT 4.37±0.23; cKO 3.93±0.43), Kcnj5 (WT 5.68±0.29; cKO 4.75±0.42), Cacna1c (WT

8.09±0.17; cKO 7.66±0.25), Cacna1g (WT 7.16±0.19; cKO 7.09±0.41) and Cacna1h (cWT5.79±0.15; cKO 6.03±0.32). There are no significant differences between the expression values for the ion channel transcripts (P>0.05, one way ANOVA with a Sidak's multiple comparison test).

DISCUSSION

Using a novel murine model we have deleted the K_{ATP} channel subunit Kir6.1 in the SAN. Uniquely, our data indicate that Kir6.1 underlies a K_{ATP} current in a proportion of SAN cells and influences repolarisation during the spontaneous action potential. This leads to mice having a bradycardic phenotype with episodes of sinus arrest in some mice, changes intrinsic to the SAN. Furthermore, the impaired adaptive responses of the SAN to hypoxia suggest the K_{ATP} channel promotes protection in these conditions. Our studies define a novel and little appreciated contributor to mammalian pacemaking.

Comparatively little literature exists on the nature of K_{ATP} channels in the SAN. In rabbit SAN cells the potassium channel openers pinacidil and cromakalim abolished pacemaker activity through membrane hyperpolarisation (18). Electrophysiological studies identified an ATP-sensitive current with a unique single channel conductance of ~50 pS rather than one closer to the 80 pS found for channels in ventricular cells (18). In mice with global genetic deletion of Kir6.2 the SAN in the intact perfused heart no longer responded to hypoxia with an increase in coupling length (13). Our data show that a prominent K_{ATP} current could be demonstrated in ~50% of murine SAN myocytes. This is perhaps not surprising as the SAN is a heterogeneous structure and a number of different cell types and regions can be distinguished (19,20). In these studies, the number of cells containing K_{ATP} currents was significantly reduced (yet not wholly abolished) in cKO mice indicating that Kir6.1 is a major contributor to these membrane currents. The single-channel conductance observed by Han and colleagues is closer to that reported for Kir6.1 containing complexes or that for various heteromultimers between Kir6.1 and Kir6.2 (18,21). The pharmacology

is also interesting with diazoxide more frequently activating these currents whilst tolbutamide as well as glibenclamide can inhibit the responses. This is more representative of SUR1 containing K_{ATP} channel complexes than SUR2, though diazoxide can act on SUR2B containing hetero-octamers (22). SUR1 containing K_{ATP} channels are already known to be present in murine atrial myocytes (23). In cKO mice there was an increase in Kir6.2 expression as assessed by RT-qPCR but not in SUR1 or SUR2 expression. Furthermore, K_{ATP} currents were essentially abolished with no response to diazoxide and only a very few cells, comparable with controls, responding to pinacidil. Thus the increased expression of Kir6.2 mRNA does not have prominent functional sequelae.

The cKO mice are clearly bradycardic when assayed by three independent assays: single cell, *ex-vivo* and *in-vivo* studies. In the latter studies, no evidence was found supporting changes in autonomic or hormonal influences on heart rate in the cKO mice. In other words, the process observed was solely intrinsic to the SA node, as would be expected from the specificity of expression of the cre recombinase.

Our action potential recordings demonstrate an increase in action potential duration particularly prominent during the early stages of repolarisation. Thus, even under resting conditions and without metabolic challenge, Kir6.1 containing K_{ATP} channels are active and contribute to potassium currents involved in shaping the SAN action potential. Furthermore, the maximum diastolic depolarisation and resting membrane potential were not prominently changed in knockout animals. The time-to-peak depolarisation was also delayed in the cKO mice. The net upshot of these cumulative effects is a prolongation of the action potential. Given an equivalent or unchanged time-period for diastolic depolarisation, a consequence would be to increase the SAN cycle length and thus decrease heart rate.

K_{ATP} currents generated by Kir6.1 containing subunits are actually outwardly rectifying (see above). However currents do not deactivate with hyperpolarisation, as

would a classic voltage-gated potassium channel, and it is surprising that they do not have a significant influence on the pacemaker depolarisation. It is known that cAMP signalling is highly developed in the SAN (24) and it is possible that phasic oscillations in PKA activity might amplify the K_{ATP} current during repolarisation. PKA is known to prominently regulate Kir6.1 containing channel complexes(25). However there is precedent for analogous observations in the literature: deletion of the gene encoding TREK-1, a background potassium current, led to sinus bradycardia and pauses (26).

The HCN4 promoter driven *cre* is also active in other regions of the conduction system. Although a formal investigation of this fell outside of the scope of this study, an increase in PR interval on the ECG reflective of delayed AV nodal conduction was observed in these animals. This implies that Kir6.1 also plays a role in the physiological function of the AV node. Indeed, gain of function mutations in the Kir6.1 subunit found in patients with Cantu syndrome and mouse models with Kir6.1 gain of function show AV conduction abnormalities (27,28).

In the global Kir6.1 knockout mouse one of the major contributors to premature death is sudden cardiac death due to bradyarrhythmia resulting from sinus arrest and heart block (14,15). Selected cKO mice displayed features of this phenomenon, but not as prominently as in the global knockouts. Opening of K_{ATP} channels can contribute to cellular protection in several pathological conditions (1,29). We therefore examined the response of the SAN to hypoxia in *ex-vivo* intact hearts, using sinus nodal recovery from burst pacing, (SNRT) as a comparison metric. In wildtype littermate controls the SNRT was prolonged by hypoxic challenge whilst in the cKO mice this did not occur. It is plausible that this response by the SAN is protective as it allows some degree of electrical silencing in conditions of metabolic challenge. The electrical silencing likely occurs through action potential failure due to overwhelming repolarising currents. This will prevent cellular calcium overload and cell death. The observed hypoplasia of the SA node and increased expression of profibrotic markers support the

hypothesis of cell death and fibrosis in cKO mice. It is difficult to unambiguously separate the functional effects of a direct effect of Kir6.1 deletion and the pathological changes seen in SAN on SAN electrophysiology. We think both contribute however it is worth noting that we have performed single cell studies on SAN myocytes where a reduced spontaneous firing rate is present in cKO mice and the relative change in heart rate in the knockout is similar to that in the *ex-vivo* and *in-vivo* studies. It is also possible that the fibrotic process leads to remodelling of ion channel expression in the SAN. Thus we examined the expression of a selected number of ion channels in the SAN using RT-qPCR. We did not find prominent changes in expression between wildtype control SAN cells and those with deletion of Kir6.1.

The more severe electrophysiological phenotype seen in global Kir6.1 knockout mice can be explained by likely episodes of coronary vasospasm leading to hypoxia in the SAN combining with failures of appropriate protective responses. The phenotype in the cKO mice is milder and sinus arrest occurs in only a limited number of mice. However, the primacy of the cardiac electrophysiology effect is supported by the observation that a pure vascular phenotype, as in a murine line with specific smooth muscle deletion, did not display a bradycardiac phenotype under resting conditions or with ergonovine (15). It is interesting that sudden infant death syndrome has been associated with loss of function mutations in KCNJ8 (30).

This study is the first to formally define the role of Kir6.1 in the sinus node, and significantly adds to the understanding of the complexities of sinus node physiology. However, there are several limitations to this study. First, this study investigated the murine SAN given that cre/loxP technology is as yet not easily replicated in other species. Mutations in Kir6.1 have been implicated in causing atrial fibrillation and early repolarisation syndromes in man (31,32). However there are data indicating that Kir6.1 may be expressed more widely in murine cardiac tissue than in man for example (33) and this may confound translation to human disease. Second, although we found evidence

for the cellular protective effects of Kir6.1, we have not performed long term aging studies that may be required to fully define the precise molecular effects on these pathways.

In conclusion, we show that K_{ATP} channels constituted of Kir6.1 are present in SAN and influence repolarisation. Cycle length is prolonged resulting in bradycardia in cKO mice. In addition, these channels may also protect against sinus node dysfunction for example during hypoxic conditions.

EXPERIMENTAL PROCEDURES

Animal husbandry - All experiments were conducted in accordance with the Guide for the Care and Use of Laboratory Animals published by the British Home Office and the US National Institutes of Health (NIH Publication No. 85-23, revised 1996). The animal work was approved by the QMUL Animal Welfare and Ethical Review Body and covered by UK Home Office project licences PPL/6732 and PPL/7665.

Generation of conduction system-specific Kir6.1 KO mice - Kir6.1 flx/wt mice were generated in our lab in collaboration with Genoway (Lyon, France; project number genOway/EV/TIN1- *Kcnj8* 070206). The generation of these mice has been described in detail previously (15). Conduction system-specific Kir6.1 KO mice were generated by crossing mice with a conduction system-specific cre, into which the tamoxifen-inducible Cre-ER^{T2} had been ‘knocked-in’ into the HCN4 locus (HCN4-KiT cre) (17), with Kir6.1 homozygous floxed (Kir6.1(flX/flX)) mice. This generated HCN4cre+ Kir6.1 flX/flX (cKO) mice and HCN4cre- Kir6.1 flX/flX littermate controls. Recombination was induced with 1mg/day/25g mouse tamoxifen (Sigma-Aldrich) administration for 5 days (I.P).

Genotyping - DNA was extracted from mouse ear biopsies by proteinase K digestion. The presence of the Kir6.1 floxed allele was confirmed using PCR with the following primer set: sense 5'-GAGATCTTAAGTCTGAGGACC AACA-3' and antisense 5'-AGCGAAGAACTGCTTCCTGTTTATT AAG-3' yielding a WT band of 474 bp and a floxed allele band of 600 bp. PCR cycle

conditions were denaturation at 94 °C for 2 minutes, 35 cycles of 94 °C for 30 secs, 63 °C for 30 secs, 68 °C for 1 minute, extension at 68 °C for 8 minutes. The presence of the cre recombinase gene in the Kir6.1 conditional knock-out line was determined using the following primer set: sense 5'-CCAATTTACTGACCGTACACC-3' and antisense 5'-GTTTCACTATCCAGGTTACGG-3' yielding a band of 900 bp in cre positive mice and no band in cre negative mice. PCR cycle conditions were denaturation at 94 °C for 2 minutes, 35 cycles of 94 °C for 1 minute, 60 °C for 1 minute, 72 °C for 1 minute, extension at 72 °C for 5 minutes. Both the floxed and cre PCRs used Taq polymerase (NEB, UK).

Quantitative real-time PCR (qRT-PCR)- Total RNA was extracted from mouse tissues using the RNAeasy kit from Qiagen. Total RNA was DNase I treated and reverse-transcribed using the High Capacity cDNA Reverse Transcription Kit (Applied Biosystems). 50 ng of cDNA was used for qRT-PCR, which was performed using customised Taqman gene expression assays (Applied Biosystems). We used the commercially available probes for all the genes as listed below: Mm00434620_m1 for *Kcnj8* (Kir6.1), Mm00440050_s1 for *Kcnj11* (Kir6.2), Mm01701349_m1 for *Abcc8* (SUR1), Mm00441638_m1 for *Abcc9* (SUR2), Mm00801666_m1 for *Col1a1* (Collagen type I), Mm01254476_m1 for *Col3a1* (Collagen type III), Mm01192933_g1 for *Ctgf* (Connective tissue growth factor), Mm01178820_m1 for *Tgfb1* (Transforming growth factor β 1), Mm00436955_m1 for *Tgfb2* (Transforming growth factor β 2), Mm01176086_m1 for *Hcn4* (HCN4), Mm00468832_m1 for *Hcn1* (HCN1), Mm004865672_m1 for *Cacna1g* (Cav3.1), Mm004382_m1 for *Cacn1h* (Cav3.2), Mm01188822_m1 for *Cacn1c* (Cav1.2), Mm00434618_m1 for *Kcnj3* (Kir3.1), Mm01175829_m1 for *Kcnj5* (Kir3.4) Each gene was assayed in triplicate. Relative expression was calculated by using the comparative C_T method normalised to GAPDH. Final data are presented as a relative change compared to control.

Isolation of SAN myocytes - SAN myocytes were isolated using the method of Mangoni and Nargeot (34). Briefly, mice were injected with heparin sodium (250 IU) and anaesthetised with a combination of ketamine (0.1 mg/g)/xylazine (0.01 mg/g). The hearts were rapidly excised and the SAN dissected and placed in Tyrode's solution consisting of (in mM); 140 NaCl, 5.4 KCl, 1.8 CaCl₂, 1 MgCl₂, 5 HEPES-NaOH, and 5.5 D-glucose (adjusted to pH 7.4 with NaOH). The SAN was then placed in low Mg²⁺/Ca²⁺ solution containing (in mM); 140 NaCl, 5.4 KCl, 0.5 MgCl₂, 0.2 CaCl₂, 1.2 KH₂PO₄, 50 taurine, 5.5 D-glucose, 1.0 mg/ml BSA, and 5.0 HEPES-NaOH (adjusted to pH 6.9 with NaOH). The tissue was digested with 1 mg/mL Collagenase Type II (Worthington), 1 mg/mL Protease (Sigma-Aldrich), 1 mg/mL BSA (Sigma-Aldrich) and 200 μ M CaCl₂ for ~20 mins at 37°C with consistent agitation with a fire-polished Pasteur pipette. The tissue was then washed 3-4 times in modified Kraft-Bruhe (KB) solution containing (in mM): 70 L-glutamic acid, 20 KCl, 80 KOH, 10 (\pm) D-b-OH-butyric acid, 10 KH₂PO₄, 10 taurine, 1 mg/ml BSA, and 10 HEPES-KOH, pH 7.4 with KOH. SAN cells were dissociated manually using a fire-polished Pasteur pipette in KB solution and allowed to rest for 5 mins prior to re-adaptation. Cells were allowed to re-adapt to physiological levels of Na⁺ and Ca²⁺ by incremental addition of a solution containing 10 mM NaCl and 1.8 mM CaCl₂ and finally normal Tyrode's solution with 1 mg/mL BSA. Re-adapted cells were stored at room temperature in storage solution containing (in mM); 100 NaCl, 35 KCl, 1.3 CaCl₂, 0.7 MgCl₂, 14 L-glutamic acid, 2 (\pm)D-b-OH-butyric acid, 2 KH₂PO₄, 2 taurine, and 1 mg/ml BSA, pH 7.4. SAN cells were plated onto 13 mm coverslips coated with laminin 30 mins prior to patch-clamp recordings.

Patch-clamp recordings from isolated SAN myocytes - Whole cell patch-clamp recordings were performed as described previously (15). Capacitance transients and series resistance in whole-cell recordings was compensated electronically by using amplifier circuitry (Axopatch 700B). Data were filtered at 1 kHz using the filter provided with the Axopatch 700B (4 pole Bessel) and sampled at 5 kHz

using a Digidata 1550 (Axon Instruments). Currents were acquired and analysed using pClamp10 (Axon Instruments). Whole-cell currents were recorded using a voltage-ramp protocol (-150 to +50 mV for 1 s). Pipette solution contained (mM); 107 KCl, 1 MgCl₂, 10 EGTA and 10 HEPES with 3 MgATP and 1 Na₂ADP, pH 7.2 using KOH. The bath solution contained (mM); 137 NaCl, 5.4 KCl, 1 MgCl₂, 1.8 CaCl₂, 5 Glucose, 10 HEPES, pH 7.4 using NaOH. Drugs were applied to the bath using a gravity-driven perfusion system. Whole-cell action potentials were recorded using the current-clamp configuration. The pipette solution for current-clamp recordings contained (mM); 110 K-Gluconate, 20 KCl, 10 HEPES, 0.05 EGTA, 0.5 MgCl₂, 5 MgATP, 0.3 Na₂-GTP, 5 Na₂-phosphocreatine, pH 7.4 using KOH. Data was initially analysed using Clampfit 10 (Axon Instruments).

Masson's Trichrome Staining - Trichrome staining was used to distinguish between muscle, collagen and connective tissue in serial 10 μM SAN sections embedded in paraffin. We used the Sigma-HT15 Trichrome Stain (Masson) Kit as per the manufacturer's instructions (Sigma-Aldrich).

ECG Telemetry - Briefly, recording leads were tunnelled subcutaneously in a conventional lead II ECG configuration connected to a telemetry device (TA-F10, Data Sciences International (DSI), Netherlands) implanted either subcutaneously or intra-abdominally. Surface ECG was continuously recorded via radio-telemetry after 2-weeks post-operative recovery. To record standard surface ECG parameters, consecutive individual ECG complexes recorded over 2 minutes during sinus rhythm at high sampling frequency (2 kHz) were analysed using Ponemah P3 plus analysis software (DSI, Netherlands). Diurnal variation of heart rate was measured by averaging heart rate over a 12 hour period (7 am to 7 pm (day) and 7 pm to 7 am (night)) corresponding to the light/dark cycle in the animal facility over at least a 48 hr period of recording.

Analysis of Heart Rate Variability - Changes in the R-R interval variability were analysed using the heart rate variability module (HRV) in LabChart v7.0 (AD Instruments). ECG

recordings taken at a low activity period (12pm-2pm) were analysed using power spectral analysis as described previously (35). R-waves were detected using a threshold-sensing algorithm and ectopic beats were excluded from the analysis. Fast Fourier transformation was performed using 1024 spectral points and a half overlap within a Welch window and power spectral density plots determined. The total power (TP) (s²/Hz) was calculated as the integral sum of total variability after Fourier transformation over the frequency range 0-4.0 Hz. Cut-off frequencies determined to be accurate for mice were used to divide the signal into three components, very low frequency (VLF: 0.0 - 0.4 Hz), low frequency (LF: 0.4 - 1.5 Hz), and high frequency (HF: 1.5 - 4.0 Hz). Data from segments was also normalized to exclude VLF. Normalized low frequency (nLF) = LF/(TP-VLF) x 100 and normalized high frequency (nHF) = HF/(TP-VLF) x 100.

Multi-Electrode-Array (MEA) Recordings - MEA recordings were taken from atrial/SAN preparations and from the intact heart. We used 2 types of MEAs to record spontaneous electrical activity (field potentials) from in vitro atrial preparations (60-electrode MEA, 60pMEA200/30iR-Ti & MEA2100 system Multi Channel Systems, Reutlingen, Germany), and the intact heart (32 electrodes flexMEA, Multi Channel Systems). Details of electrophysiological recordings with the MEA2100 system have been described previously (36). Briefly, the right atrial appendage and SA node were carefully and quickly dissected from the heart following excision and placed on the MEA dish and secured for good contact with electrodes with a holder. Tissue was continuously perfused with warm (37°C) and oxygenated (95% O₂/5% CO₂) Krebs solution (consisting of mM; NaCl 118, KCl 4.75, MgSO₄·7H₂O 1.19, NaHCO₃ 25, KH₂PO₄ 1.19, D-glucose 5 mM, CaCl₂ 1.4 and sodium pyruvate 2 mM). The tissue was allowed to equilibrate for 30 minutes prior to recording of spontaneous extracellular field potentials using MC Rack software (v4.6.2, Multi Channel Systems).

For experiments on intact isolated heart preparations, hearts were excised as above and quickly cannulated via the aorta and

mounted onto a modified Langendorff setup. Hearts were continuously retrogradely perfused with Krebs (as above). The flexMEA was placed on the boundary of the right ventricle and right atria allowing for measurement of spontaneous electrical signals from both atria and ventricles using MC Rack software. Sinus node recovery time (SNRT) was measured using the flexMEA and a unipolar electrode to pace at S1S1 cycle lengths of 100 ms. SNRT was measured from

the last pacing spike to the first atrial signal. Data was analysed using LabChart v7 and Clampfit v10.

Statistical Analysis – Data are presented as mean \pm SEM. Data was analysed using Microsoft Excel (Microsoft), Microcal Origin and GraphPad Prism. Student's t test and ANOVA were used to compare means where appropriate. $P \leq 0.05$ was taken to be significant.

Acknowledgements: We are grateful to Dr Sonia Sebastian and Dr Keat-Eng Ng for technical assistance.

Sources of funding: This research was supported by the British Heart Foundation (RG/15/15/31742) and was facilitated by the NIHR Biomedical Research Centre at Barts.

Disclosures: None and the authors have no conflicts of interest.

Author Contribution: QA and AT devised the research and wrote the paper. AT raised the funding for the research. QA, MF, DM, LO, YL and NA performed the research. AL provided a key experimental resource. All authors discussed and approved the paper. All authors discussed and approved the paper.

Reference List

1. Tinker, A., Aziz, Q., and Thomas, A. (2014) The role of ATP-sensitive potassium channels in cellular function and protection in the cardiovascular system. *Br. J. Pharmacol.* **171**, 12-23
2. Noma, A. (1983) ATP-regulated K⁺ channels in cardiac muscle. *Nature* **305**, 147-148
3. Ashcroft, F. M., Kakei, M., Kelly, R. P., and Sutton, R. (1987) ATP-sensitive K⁺ channels in human isolated pancreatic B-cells. *FEBS Lett.* **215**, 9-12
4. Rorsman, P. and Braun, M. (2013) Regulation of insulin secretion in human pancreatic islets. *Annu. Rev. Physiol* **75**, 155-179
5. Inagaki, N., Gonoi, T., Clement, J. P. 4., Namba, N., Inazawa, J., Gonzalez, G., Aguilar Bryan, L., Seino, S., and Bryan, J. (1995) Reconstitution of IKATP: an inward rectifier subunit plus the sulfonylurea receptor. *Science* **270**, 1166-1170
6. Inagaki, N., Gonoi, T., Clement, J. P., Wang, C. Z., Aguilar Bryan, L., Bryan, J., and Seino, S. (1996) A family of sulfonylurea receptors determines the pharmacological properties of ATP-sensitive K⁺ channels. *Neuron* **16**, 1011-1017
7. Aguilar Bryan, L., Nichols, C. G., Wechsler, S. W., Clement, J. P. 4., Boyd, A. E., Gonzalez, G., Herrera Sosa, H., Nguy, K., Bryan, J., and Nelson, D. A. (1995) Cloning of the beta cell high-affinity sulfonylurea receptor: a regulator of insulin secretion. *Science* **268**, 423-426
8. Li, N., Wu, J. X., Ding, D., Cheng, J., Gao, N., and Chen, L. (2017) Structure of a Pancreatic ATP-Sensitive Potassium Channel. *Cell* **168**, 101-110
9. Martin, G. M., Yoshioka, C., Rex, E. A., Fay, J. F., Xie, Q., Whorton, M. R., Chen, J. Z., and Shyng, S. L. (2017) Cryo-EM structure of the ATP-sensitive potassium channel illuminates mechanisms of assembly and gating. *Elife*. **6**, pii: e31054
10. Zingman, L. V., Hodgson, D. M., Bast, P. H., Kane, G. C., Perez-Terzic, C., Gumina, R. J., Pucar, D., Bienengraeber, M., Dzeja, P. P., Miki, T., Seino, S., Alekseev, A. E., and Terzic, A. (2002) Kir6.2 is required for adaptation to stress. *Proc. Natl. Acad. Sci. U. S. A* **99**, 13278-13283
11. Bao, L., Kefaloyianni, E., Lader, J., Hong, M., Morley, G., Fishman, G. I., Sobie, E. A., and Coetzee, W. A. (2011) Unique properties of the ATP-sensitive K(+) channel in the mouse ventricular cardiac conduction system. *Circ. Arrhythm. Electrophysiol.* **4**, 926-935
12. Flagg, T. P., Kurata, H. T., Masia, R., Caputa, G., Magnuson, M. A., Lefer, D. J., Coetzee, W. A., and Nichols, C. G. (2008) Differential structure of atrial and ventricular KATP: atrial KATP channels require SUR1. *Circ. Res.* **103**, 1458-1465
13. Fukuzaki, K., Sato, T., Miki, T., Seino, S., and Nakaya, H. (2008) Role of sarcolemmal ATP-sensitive K⁺ channels in the regulation of sinoatrial node automaticity: an evaluation using Kir6.2-deficient mice. *J. Physiol* **586**, 2767-2778
14. Miki, T., Suzuki, M., Shibasaki, T., Uemura, H., Sato, T., Yamaguchi, K., Koseki, H., Iwanaga, T., Nakaya, H., and Seino, S. (2002) Mouse model of Prinzmetal angina by disruption of the inward rectifier Kir6.1. *Nat. Med.* **8**, 466-472

15. Aziz, Q., Thomas, A. M., Gomes, J., Ang, R., Sones, W. R., Li, Y., Ng, K. E., Gee, L., and Tinker, A. (2014) The ATP-Sensitive Potassium Channel Subunit, Kir6.1, in Vascular Smooth Muscle Plays a Major Role in Blood Pressure Control. *Hypertension* **64**, 523-529
16. Aziz, Q., Li, Y., Anderson, N., Ojake, L., Tsisanova, E., and Tinker, A. (2017) Molecular and functional characterization of the endothelial ATP-sensitive potassium channel. *J. Biol. Chem.* **292**, 17587
17. Hoesl, E., Stieber, J., Herrmann, S., Feil, S., Tybl, E., Hofmann, F., Feil, R., and Ludwig, A. (2008) Tamoxifen-inducible gene deletion in the cardiac conduction system. *J. Mol. Cell Cardiol.* **45**, 62-69
18. Han, X., Light, P. E., Giles, W. R., and French, R. J. (1996) Identification and properties of an ATP-sensitive K⁺ current in rabbit sino-atrial node pacemaker cells. *J. Physiol* **490** (Pt 2), 337-350
19. Boyett, M. R., Dobrzynski, H., Lancaster, M. K., Jones, S. A., Honjo, H., and Kodama, I. (2003) Sophisticated architecture is required for the sinoatrial node to perform its normal pacemaker function. *J. Cardiovasc. Electrophysiol.* **14**, 104-106
20. Monfredi, O., Dobrzynski, H., Mondal, T., Boyett, M. R., and Morris, G. M. (2010) The anatomy and physiology of the sinoatrial node--a contemporary review. *Pacing Clin. Electrophysiol.* **33**, 1392-1406
21. Cui, Y., Giblin, J. P., Clapp, L. H., and Tinker, A. (2001) A mechanism for ATP-sensitive potassium channel diversity: functional coassembly of two pore forming subunits. *Proc. Natl. Acad. Sci. U. S. A* **98**, 729-734
22. Giblin, J. P., Cui, Y., Clapp, L. H., and Tinker, A. (2002) Assembly limits the pharmacological complexity of ATP-sensitive potassium channels. *J. Biol. Chem.* **277**, 13717-13723
23. Glukhov, A. V., Flagg, T. P., Fedorov, V. V., Efimov, I. R., and Nichols, C. G. (2010) Differential K(ATP) channel pharmacology in intact mouse heart. *J. Mol. Cell Cardiol.* **48**, 152-160
24. Lakatta, E. G., Maltsev, V. A., and Vinogradova, T. M. (2010) A coupled SYSTEM of intracellular Ca²⁺ clocks and surface membrane voltage clocks controls the timekeeping mechanism of the heart's pacemaker. *Circ. Res.* **106**, 659-673
25. Quinn, K. V., Giblin, J. P., and Tinker, A. (2004) Multisite Phosphorylation Mechanism for Protein Kinase A Activation of the Smooth Muscle ATP-Sensitive K⁺ Channel. *Circ. Res.* **94**, 1359-1366
26. Unudurthi, S. D., Wu, X., Qian, L., Amari, F., Onal, B., Li, N., Makara, M. A., Smith, S. A., Snyder, J., Fedorov, V. V., Coppola, V., Anderson, M. E., Mohler, P. J., and Hund, T. J. (2016) Two-Pore K⁺ Channel TREK-1 Regulates Sinoatrial Node Membrane Excitability. *J. Am. Heart Assoc.* **5**, e002865
27. Levin, M. D., Zhang, H., Uchida, K., Grange, D. K., Singh, G. K., and Nichols, C. G. (2015) Electrophysiologic consequences of KATP gain of function in the heart: Conduction abnormalities in Cantu syndrome. *Heart Rhythm.* **12**, 2316-2324

28. Levin, M. D., Singh, G. K., Zhang, H. X., Uchida, K., Kozel, B. A., Stein, P. K., Kovacs, A., Westenbroek, R. E., Catterall, W. A., Grange, D. K., and Nichols, C. G. (2016) K(ATP) channel gain-of-function leads to increased myocardial L-type Ca(2+) current and contractility in Cantu syndrome. *Proc. Natl. Acad. Sci. U. S. A* **113**, 6773-6778
29. Zingman, L. V., Alekseev, A. E., Hodgson-Zingman, D. M., and Terzic, A. (2007) ATP-sensitive potassium channels: metabolic sensing and cardioprotection. *J. Appl. Physiol* **103**, 1888-1893
30. Tester, D. J., Tan, B. H., Medeiros-Domingo, A., Song, C., Makielski, J. C., and Ackerman, M. J. (2011) Loss-of-function mutations in the KCNJ8-encoded Kir6.1 K(ATP) channel and sudden infant death syndrome. *Circ. Cardiovasc. Genet.* **4**, 510-515
31. Delaney, J. T., Muhammad, R., Blair, M. A., Kor, K., Fish, F. A., Roden, D. M., and Darbar, D. (2012) A KCNJ8 mutation associated with early repolarization and atrial fibrillation. *Europace*. **14**, 1428-1432
32. Barajas-Martinez, H., Hu, D., Ferrer, T., Onetti, C. G., Wu, Y., Burashnikov, E., Boyle, M., Surman, T., Urrutia, J., Veltmann, C., Schimpf, R., Borggrefe, M., Wolpert, C., Ibrahim, B. B., Sanchez-Chapula, J. A., Winters, S., Haissaguerre, M., and Antzelevitch, C. (2012) Molecular genetic and functional association of Brugada and early repolarization syndromes with S422L missense mutation in KCNJ8. *Heart Rhythm*. **9**, 548-555
33. Fedorov, V. V., Glukhov, A. V., Ambrosi, C. M., Kosteki, G., Chang, R., Janks, D., Schuessler, R. B., Moazami, N., Nichols, C. G., and Efimov, I. R. (2011) Effects of KATP channel openers diazoxide and pinacidil in coronary-perfused atria and ventricles from failing and non-failing human hearts. *J. Mol. Cell Cardiol.* **51**, 215-225
34. Mangoni, M. E. and Nargeot, J. (2001) Properties of the hyperpolarization-activated current (I_f) in isolated mouse sino-atrial cells. *Cardiovasc. Res.* **52**, 51-64
35. Zuberi, Z., Birnbaumer, L., and Tinker, A. (2008) The role of inhibitory heterotrimeric G-proteins in the control of in-vivo heart rate dynamics. *Am. J. Physiol Regul. Integr. Comp Physiol* **295**, R1822-R1830
36. Lane, J. D., Montaigne, D., and Tinker, A. (2017) Tissue-Level Cardiac Electrophysiology Studied in Murine Myocardium Using a Microelectrode Array: Autonomic and Thermal Modulation. *J. Membr. Biol.* **250**, 471-481

Table 1. Action potential parameters recorded from isolated SAN cells

AP Parameters	WT (n=15/9)	cKO (n=11/7)
RMP (mV)	-48.7 ± 2.2	-51.8 ± 2.3
MDP (mV)	-52.6 ± 1.5	-54.1 ± 2.3
Time to Peak (ms)	140.1 ± 12.0	186.6 ± 14.2*
Amplitude (mV)	65.9 ± 6.9	78.2 ± 8.4*
Peak amplitude (mV)	15.6 ± 5.5	26.6 ± 6.5
dV/dt (mV/ms)	0.4 ± 0.0	0.4 ± 0.1

RMP= resting membrane potential, MDP= maximum diastolic potential.
Data is shown as mean ± SEM, *P<0.05 compared to WT. n= cells/mice.

FIGURE LEGENDS

Figure 1. Generation and characterisation of the conduction system-specific knockout mouse (cKO). A, Cre-LoxP targeting strategy for the deletion of exon 2 of the *Kcnj8* gene. A targeting vector construct for *Kcnj8* with a 5' loxP site together with a FRT-flanked neomycin (Neo) selection cassette within intron 1 upstream of exon 2 and the second loxP site in intron 2 and diphtheria toxin A (DTA) negative selection marker downstream. Mice with the recombined *Kcnj8* locus were crossed with global flp-deleter mice to allow Flp-mediated excision of the neomycin selection cassette and generate Kir6.1 (+/flx) offspring. Kir6.1 (flx/flx) mice were then crossed with mice in which the cre recombinase expression is driven by a tamoxifen inducible HCN4 promoter to produce HCN4cre+ Kir6.1 (flx/flx) (cKO) mice. B, PCR of the cre recombinase (top) from mouse ear biopsies and of the floxed allele (bottom) of DNA isolated from SAN, ventricles, left atria and aorta of cKO mice before and after tamoxifen administration. C, Relative levels of expression of Kir6.1 (*Kcnj8*), Kir6.2 (*Kcnj11*), SUR1 (*Abcc8*) and SUR2 (*Abcc9*) in the SAN, left atria (LA) and ventricles (VT) from WT and cKO mice. The gene expression level in each case was normalized to the WT. Data is shown as mean ± S.E.M, n=5 mice, **P<0.01 compared to WT

Figure 2. Deletion of Kir6.1 in the conduction system results in loss of K_{ATP} current in SAN cells.

A, Representative time-course traces at +40 mV (right panel) and whole-cell current density-voltage traces (left panel) taken from SAN cells isolated from WT and cKO mice following tamoxifen induction showing the effects of pinacidil (Pin), diazoxide (DZX), tolbutamide (TOL) and glibenclamide (Glib). The control (Con) trace is shown in grey. Current-voltage relationships were recorded using a 1s ramp protocol (-150 mV to +50 mV) from a holding potential of -80 mV. B, Summary of the mean current-densities at +40 mV from ECs isolated from WT (top) and cKO (bottom) mice. C, Proportion of WT (n=29) and cKO (n=18) SAN cells responsive to pinacidil and/or diazoxide. D, Mean tolbutamide-sensitive current recorded from SAN cells isolated from WT and cKO mice. n=9-12 cells from 3-10 mice. Data is shown as mean ± S.E.M. *P<0.05 compared to control/WT.

Figure 3. Tamoxifen-induced Kir6.1 deletion in SAN leads to bradycardia in cKO mice.

Representative 2 lead ECG traces from conscious freely-moving WT (A) and cKO (B) mice before and after tamoxifen administration. Expanded traces (inset) show changes in PR interval before (black) and after (grey) tamoxifen administration. Mean heart rate (HR), PR and RR interval determined from ECGs recorded over a 48hr period from WT (C) and cKO (D) mice. E, Example trace from a cKO mouse showing sinus node dysfunction characterised by pronounced bradycardia and episodes of sinus pauses. F, Mean data showing the number of RR intervals greater than 200 ms in WT and cKO mice. n=7-8 mice. **P<0.01 compared to WT.

Figure 4. Heart rate variability does not contribute to the bradycardic phenotype in cKO mice.

Representative frequency domain power spectral density plots from WT (A) and cKO (B) mice. HF indicates high-frequency band (1.5–4 Hz); LF, low-frequency band (0.4–1.5 Hz); and VLF, very-low frequency band (0–0.4 Hz). C, Mean normalised data comparing VF and HF before and after tamoxifen administration in WT and cKO mice. D, Mean total power before and after tamoxifen administration in WT and cKO. Data is shown as mean ± SEM. n=5.

Figure 5. Action potential firing rate is reduced and action potential duration (APD) prolonged in isolated pacemaker cells from cKO mice. A, Representative train of spontaneous action potentials recorded from isolated WT and cKO SAN cells using whole-cell current clamp. B, Representative single action potentials from a WT (black) and cKO (grey) SAN cell. C&D, Observed spontaneous rates prior to electrophysiological recording (C) and recorded beat frequency after establishment of the whole configuration (D) in SAN cells from WT and cKO mice. E, Mean APD values for APD20 (the duration of the action potential measured at 20% of the amplitude) to APD100 for action potentials from WT and cKO SAN cells. n=11-15 cells from 7-9 mice. F, Mean APD90/50 values for APs from WT and cKO cells. G, Mean APD30-40/APD70-80 values for APs from WT and cKO cells. n=11-15 cells from 7-9 mice. Data is shown as mean \pm S.E.M. *P<0.05, **P<0.01, ***P<0.001 compared to control/WT.

Figure 6. Reduced beat frequency in intact right atrial/SAN preparations and increased SNRT in intact hearts from cKO mice. A, Representative field potentials from WT and cKO right atrial (RA) tissue with the SAN intact recorded using 2-D MEA. B, Mean beat frequency from RA/SAN tissue from WT (n=11) and cKO (n=12) mice. C, SNRT was measured using a flexMEA on isolated heart preparations. Hearts were paced for 20 s at S1S1 cycle lengths of 100 ms and defined as the time interval from the last pacing spike to the first recorded atrial activity. Hearts were challenged with hypoxia (95% N₂) and reperfusion. D, Mean basal SNRT measured from WT (n=12) and cKO (n=10) hearts. E, Mean relative SNRT during hypoxia and reperfusion in WT (n=12) and cKO (n=10) hearts. Data is shown as mean \pm SEM. *P<0.05 compared WT.

Figure 7. SANs from cKO mice are hypomorphic with increased expression of pro-fibrotic markers. Representative images of Mason's trichrome staining of SAN from WT (A) and cKO (B) mice. C, Relative expression of pro-fibrotic markers in WT and cKO SAN tissue. n=5. Data is shown as mean \pm SEM. *P<0.05, **P<0.01 compared to WT.

Figure 1

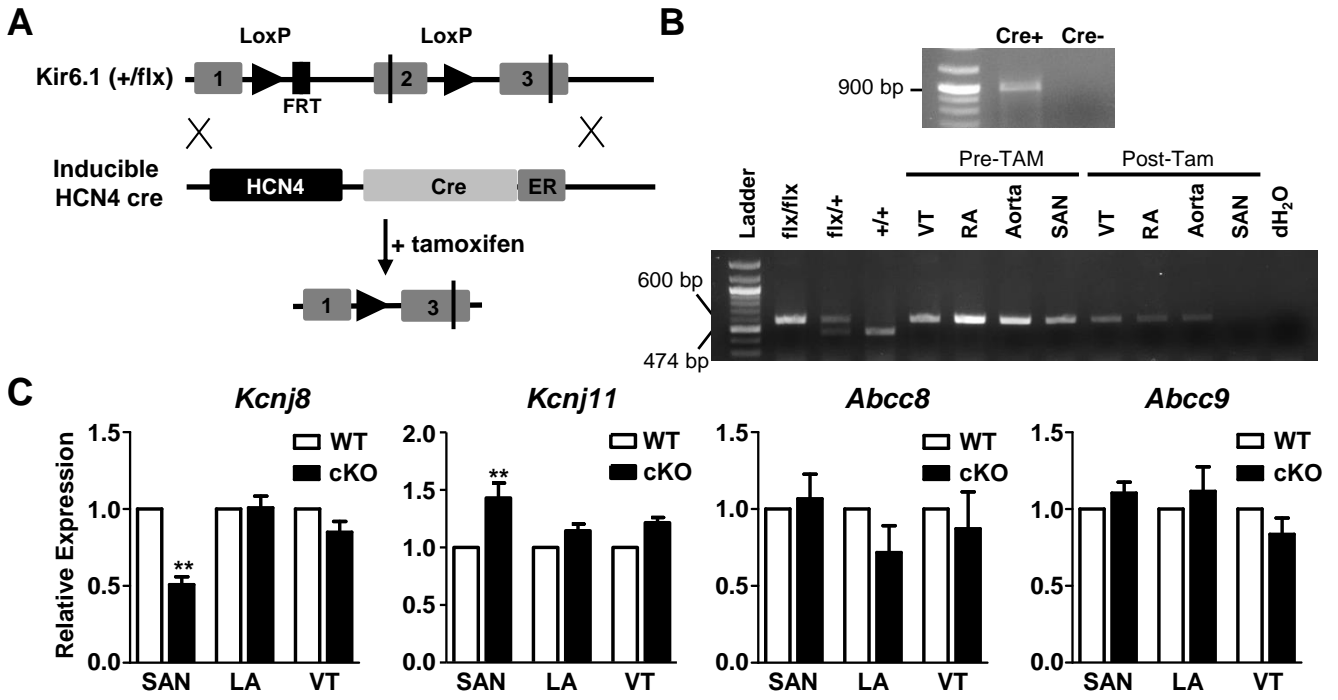


Figure 2

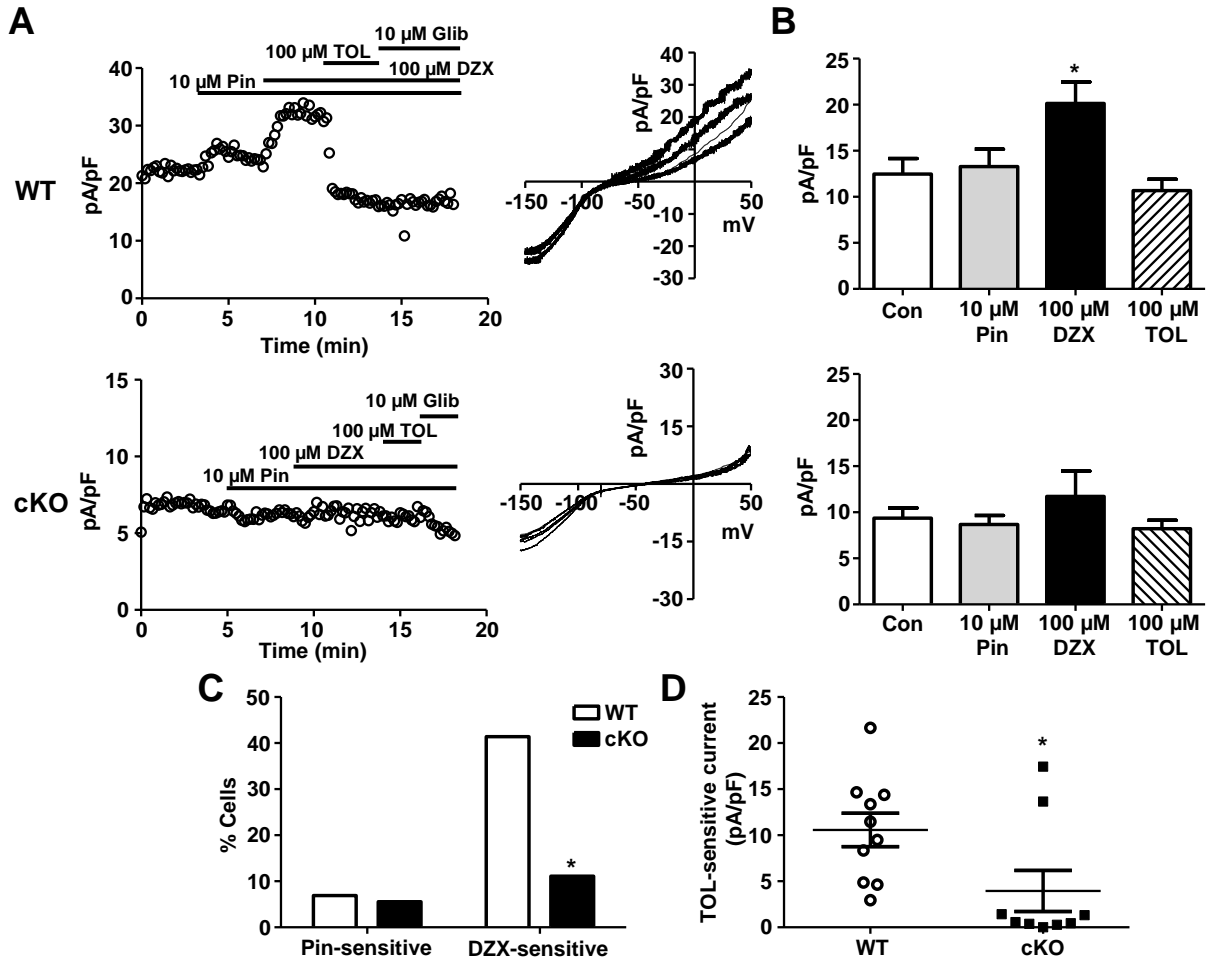


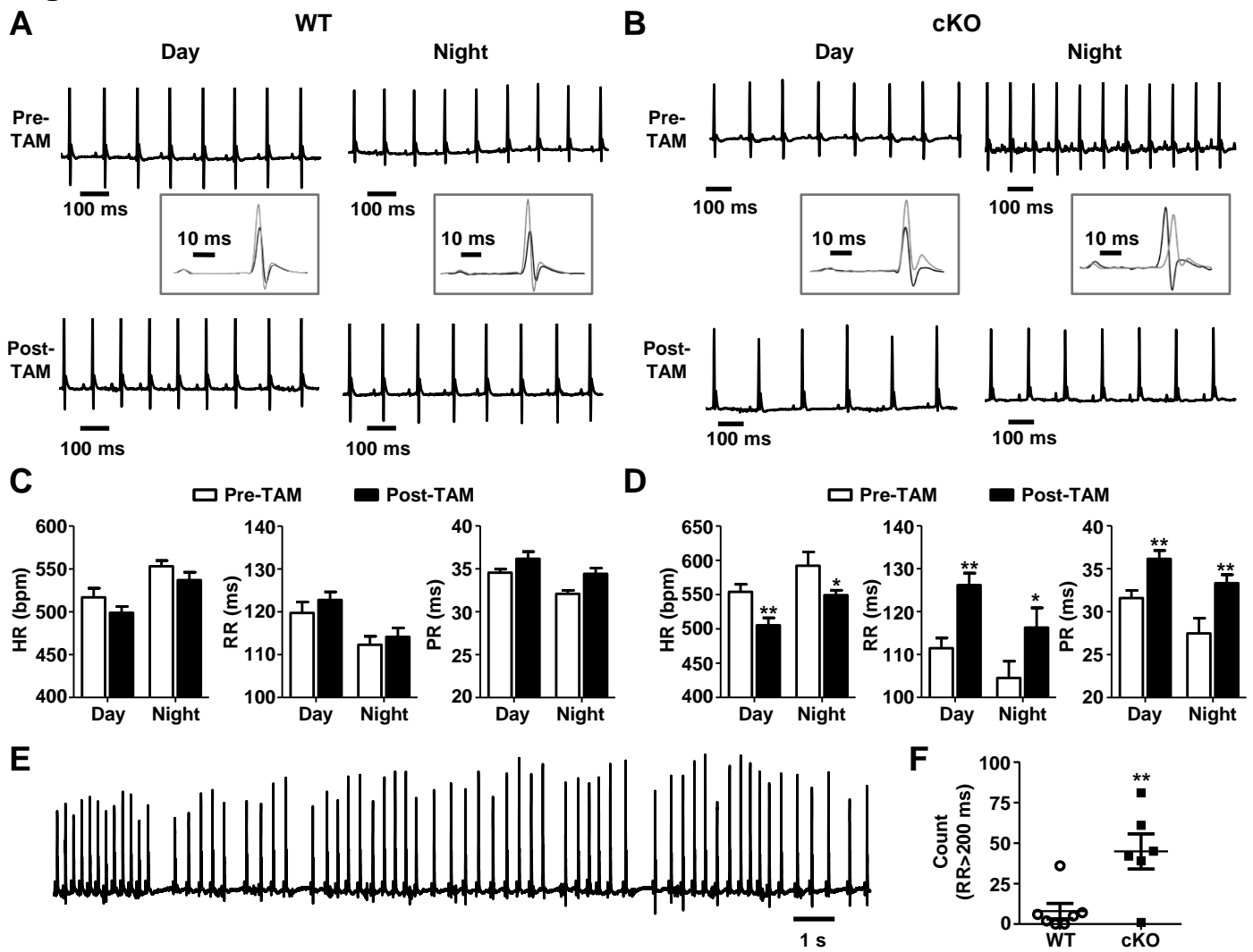
Figure 3

Figure 4

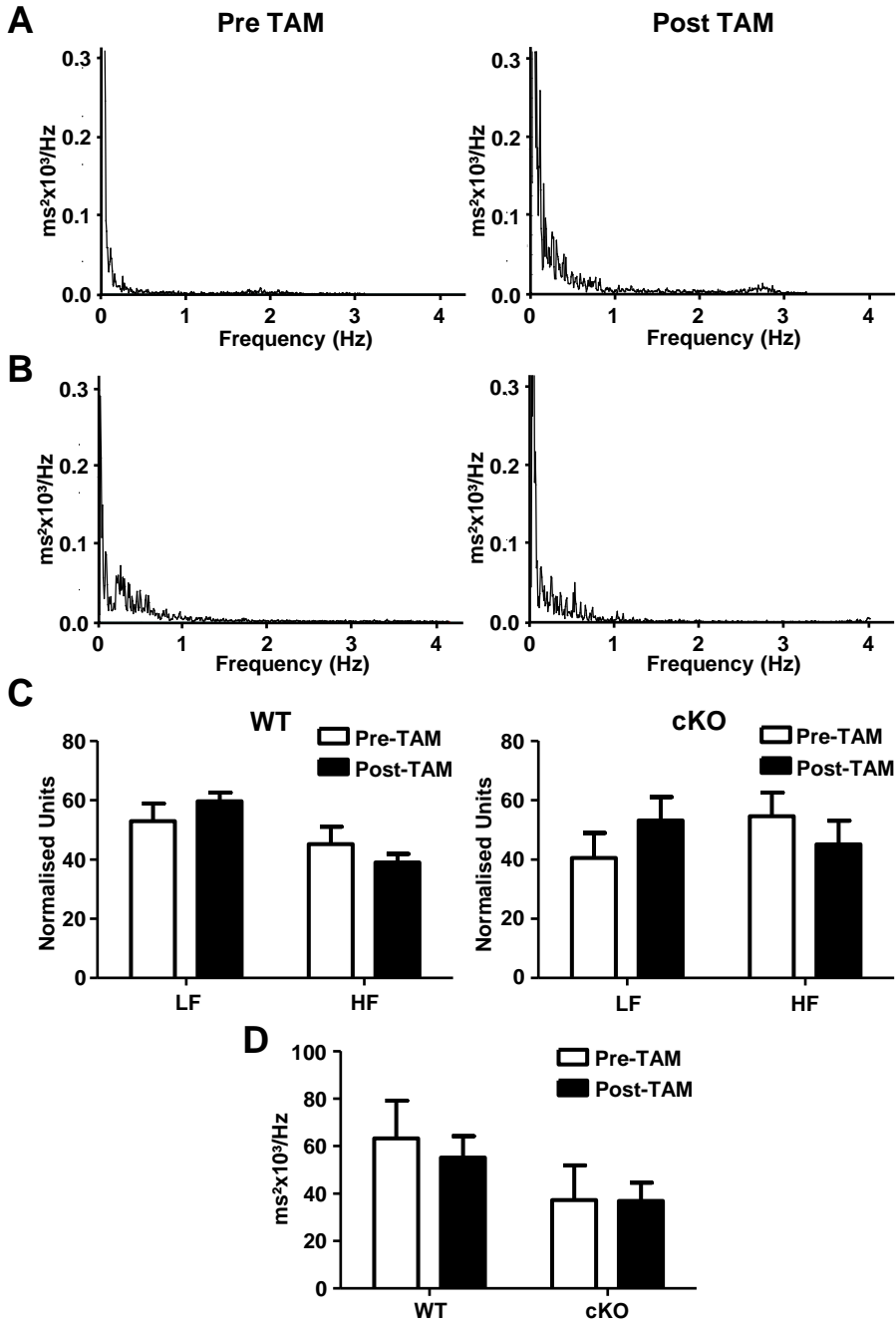


Figure 5

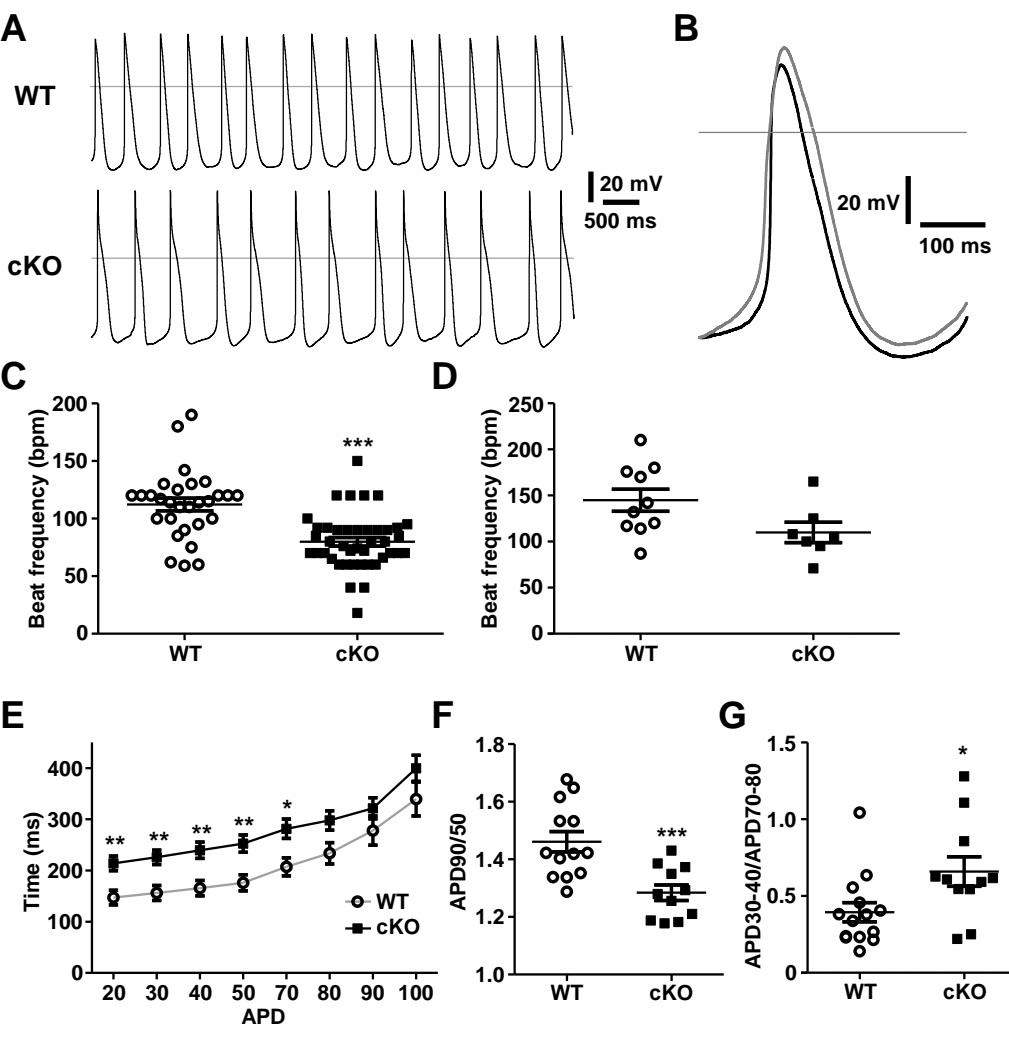
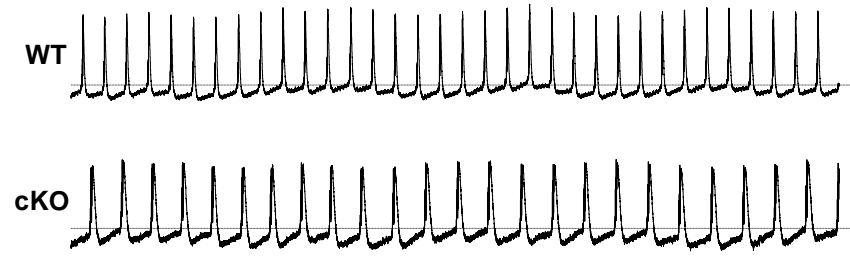
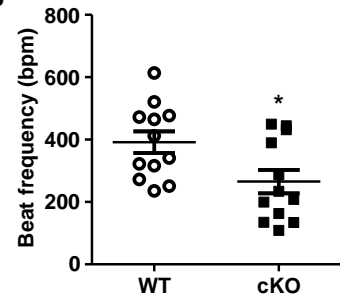


Figure 6

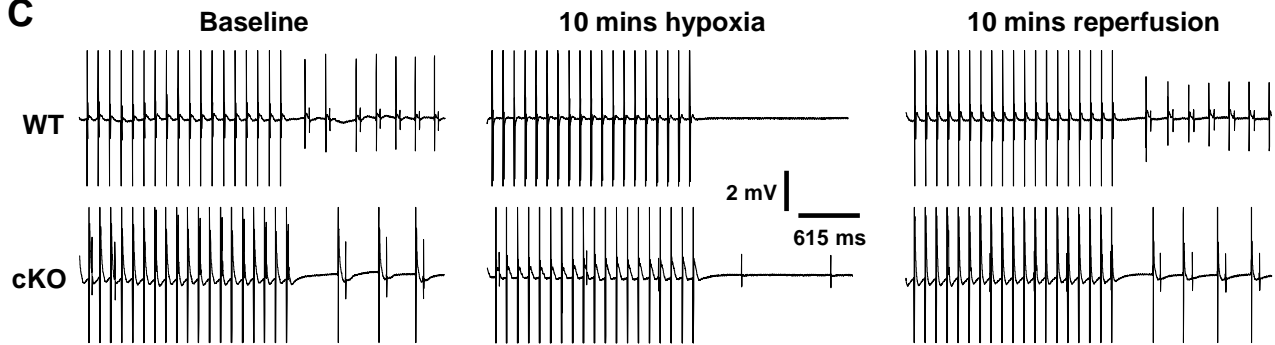
A



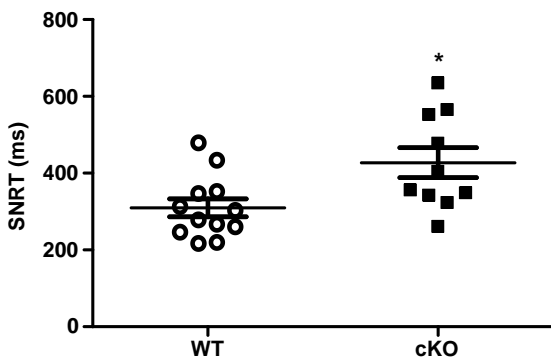
B



C



D



E

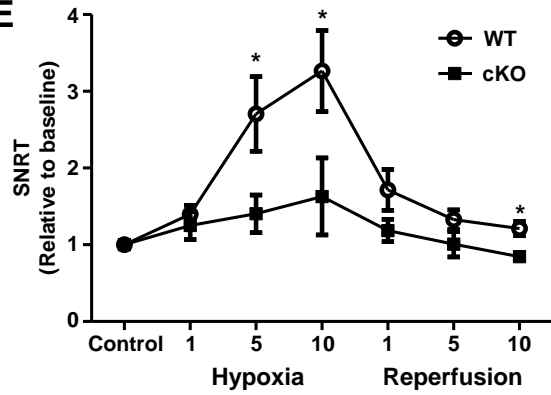
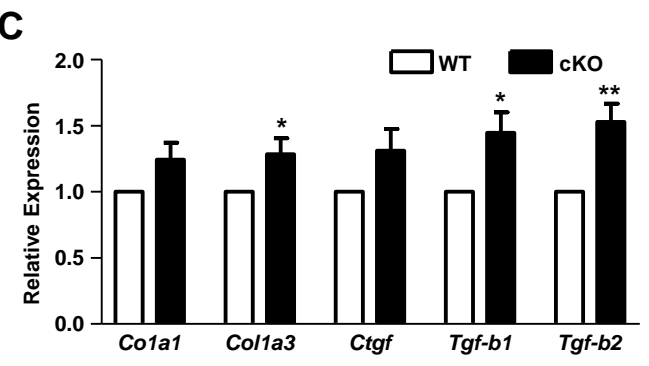
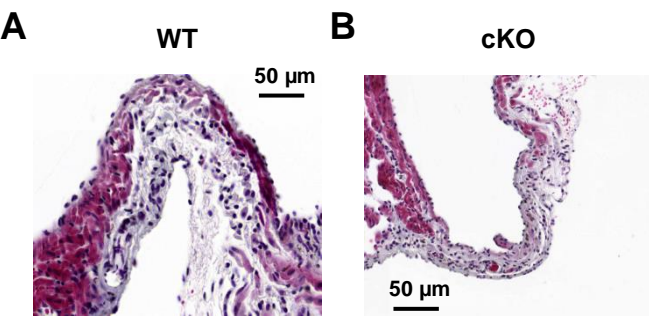


Figure 7



ATP-sensitive potassium channels in the sinoatrial node contribute to heart rate control and adaptation to hypoxia

Qadeer Aziz, Malcolm Finlay, David Montaigne, Leona Ojake, Yiwen Li, Naomi Anderson, Andreas Ludwig and Andrew Tinker

J. Biol. Chem. published online April 17, 2018

Access the most updated version of this article at doi: [10.1074/jbc.RA118.002775](https://doi.org/10.1074/jbc.RA118.002775)

Alerts:

- [When this article is cited](#)
- [When a correction for this article is posted](#)

[Click here](#) to choose from all of JBC's e-mail alerts